Title

Corrosion inhibition effects of metal cations on SUS304 in 0.5 M Cl^- aqueous solution.

Author Names

Md. Saiful ISLAM[1)], Kyohei OTANI[1)], Masatoshi SAKAIRI[2)]

Affiliations

1) Graduate School of Engineering, Hokkaido University, Kita-13, Nishi-8, Kita-ku, Sapporo, Hokkaido 060-8628, Japan.
2) Faculty of Engineering, Hokkaido University, Kita-13, Nishi-8, Kita-ku, Sapporo, Hokkaido 060-8628, Japan.

Abstract

The corrosion characteristics of SUS304 exposed to 0.5 M Cl^- aqueous solution containing different metal cations were studied with immersion tests, surface analysis and electrochemical tests. The mechanism of corrosion with metal cations was clarified by the XPS analysis results together with the hard and soft acid and base (HSAB) concept and the passive films structure. It is supposed that metal cations with large hardness make a layer by chemical bonding with the passive films. The passive films are protected by the metal cation layer from Cl^- attack, and consequently corrosion reactions are inhibited.

Keywords: Stainless steel; passive films; SEM; XPS; EIS; AFM.

1. Introduction

SUS304 is very popular and widely used in applications requiring high corrosion resistance. However, corrosion of stainless steel is a serious problem in liquid supply pipes and storage tanks, ships, bridges and many other constructions. Corrosion of stainless steel has been investigated by many researchers [1-11]. The corrosion resistance property of stainless steel mostly depends on the stability of the passive films. In corrosive environment, the re-passivation properties of the passive films provide the key to the high corrosion resistance of stainless steels [12, 13].

Corrosion of stainless steel depends on the various environmental factors. One of the important factor is presence of anions (Cl^- and SO_4^{2-}) in the aqueous solution. Cl^- plays a major role in corrosion of steel because the passive films are easily destroyed by this anion [14-18]. Corrosion reactions are initiated on the steel surface while the passive films are destroyed by Cl^- in the aqueous solution [14-20]. The passive films stability is decreased with increasing the Cl^- concentration in the aqueous solution. In other word, corrosion of steel is highly correlated with the Cl^- concentration [21-27]. There are reports that metal cations can change the corrosion behavior of steel in aqueous solution [21-29]. Islam et al. [21] studied the inhibiting effects of metal cations on mild steel corrosion in Cl^- containing aqueous solution. Otani et al. [22, 23] investigated the effects of metal cations on steel corrosion in fresh water and they found that metal cations have an ability to make a layer on the passive films and protect the film from Cl^- attack in the solution. Zhang et al. [24] studied the inhibiting effect of metal cations and reported that some metal cations (Mn^{2+}, Ni^{2+} and Zn^{2+}) effectively inhibit the intergranular stress corrosion cracking of sensitized type 304 stainless steel in SO_4^{2-} (10^{-5} kmol/m^3) containing aqueous solution. They also clarified the effects of metal cations with hardness, *X*, which is based on the hard and soft acid and base (HSAB) concept. Khedr et al. [25] studied the role of metal cations in the corrosion and corrosion

inhibition of aluminium in aqueous solutions of SO_4^{2-} and NO_3^-. O'dell et al. [28] reported that some metal cations exhibit inhibiting effects to the intergranular stress corrosion cracking of sensitized type 304 stainless steel in Cl^- containing aqueous solution. Drazic et al. [29] reported that Cd^{2+}, Mn^{2+} and Zn^{2+} inhibit the corrosion of iron in sulphuric acid solutions. Gatos [30] investigated the effects of metal cations on the corrosion of iron in acids. In some nuclear power reactors, metal cations are added into high temperature water for suppressing corrosion of the reactor component materials and avoiding accumulation of radioactive metal element [24, 31]. Therefore, it has been confirmed that metal cations affect the corrosion of stainless steel in aqueous solution [24, 32]. However, the effects of metal cations on corrosion of SUS304 in 0.5 M Cl^- aqueous solution remain unknown and the corrosion inhibition mechanism of metal cations with the passive films are not fully elucidated.

In this study, the effects of metal cations on corrosion of SUS304 in 0.5 M Cl^- aqueous solution were investigated by immersion tests, electrochemical tests, scanning electron microscope (SEM), atomic force microscope (AFM) and X-ray photoelectron spectroscope (XPS). The corrosion inhibition mechanism of metal cations with the passive films structure has also been clarified by the hardness of metal cation, *X*, based on the hard and soft acid and base (HSAB) concept.

2. Experimental

2.1 Specimens

SUS304 sheets were cut into small pieces (7 × 7 × 1 mm) and were used as specimens. In the case of electrochemical tests, a conductive wire was connected to each specimen to use as a working electrode. All the specimens were molded in epoxy resin (Struers Ltd., Epofix Resin) to carried out different tests [21]. The exposed surface of the molded specimen was grounded with SiC abrasive paper from #1000 to #4000 grit size. For immersion tests, the

specimens were taken out from the resin after polished [21]. Before performing the tests, all the specimens were cleaned in ethanol and then in highly purified water using ultrasonic bath.

2.2 Solutions

Three 0.5 M Cl^- solutions with different metal cations were used as test solutions; 0.1 mM $MgCl_2$ (Mg_{sol}), 0.1 mM $ZnCl_2$ (Zn_{sol}), and 0.1 mM $AlCl_3$ (Al_{sol}) and their Cl^- concentration was adjusted to 0.5 M by NaCl. In this experiment, 0.5 M NaCl (Na_{sol}) was used as a reference solution. Water used in this study was highly purified; distilled two times and further purified by water purifier (MILIPORE, Simplicity UV). All chemicals used in this study were special analytical grade and obtained from Kanto Chemical Co. Ltd.

Corrosion reactions are mostly depended on the pH of the aqueous solution [33, 34]. It is essential to control the pH of aqueous solution for better understanding the individual effect of metal cations on the corrosion of stainless steel. The pH of used solutions was adjusted between 5.7 and 5.8 by 0.1 M NaOH (Table 1) before the tests. The pH of the solutions before and after immersion tests were measured by the pH meter (Eutech Instruments Pte. Ltd., Cyber-Scan 6000).

2.3 Immersion tests

Specimens were immersed in the solutions at 25° C for 56 d (8 weeks). During the immersion tests, the solutions were open to the air. The mass of the specimens was measured using a micro balance (METTLER TOLEDO MX5, Pro FACT) before and after the immersion tests, and the corrosion rates were calculated from the mass change [21].

Before and after the immersion tests, the surfaces of the specimens were observed by a digital camera (Nikon D80-DSLR) and scanning electron microscope using secondary electrons imaging (SEM, JEOL Ltd., JSL6510-LA). The surface of the immersed specimens was analyzed by X-ray photoelectron spectroscope (XPS, JEOL Ltd., JPS-9200) using a monochrome Al Kα X-ray source (1486.6 eV). The diameter of specimen surface analyzed

by the XPS was 3 mm. The surface roughness was measured by atomic force microscope (AFM, SPA400) using dynamic force mode with the cantilever type, SI-DF40. Before the analysis, the immersed specimens were cleaned ultrasonically first in ethanol and then in highly purified water.

2.4 Electrochemical tests

Electrochemical tests were performed in a conventional three-electrode cell using a potentiostat (IVIUM TECHNOLOGIES, Pocketstat). Before the tests, the specimens were immersed in the solutions at 25° C for 7 d. A platinum plate and a Ag/AgCl electrode immersed in a saturated KCl solution (SSE) were used as counter and reference electrodes, respectively. The exposed surface area of working electrode in the solution was 49 mm^2. The potentiodynamic polarization measurements were carried out from immersion potential to the cathodic and anodic direction with a scan rate of 1 mV/s. The cathodic and anodic scan was started separately to obtain the individual electrochemical properties of stainless steel immersed in the solutions with metal cations. The impedance spectra were measured in a frequency range from 100 kHz to 1 mHz and a modulation amplitude of 10 mV. For the EIS curve-fitting, the IVIUM software was used. Reproducible data were obtained in all electrochemical measurements.

3. Results

3.1 Immersion tests

The appearances of solutions and specimens after immersion at 25°C for 56 d in the test solutions are shown in Fig. 1. No significant change is observed in the color of the test solutions (Fig. 1 (a)) after the immersion period. It is very difficult to identify the surface morphological difference from Fig. 1 (b) due to the extent of corrosion is very less and few amount of corrosion products may have formed.

The corrosion rates were calculated from the mass loss after immersion for 56 d in the different solutions. Fig. 2 shows the corrosion rate as a function of *X*, and the corrosion rate is gradually decreasing with increasing the value of *X*. The correlation coefficient is -0.92 indicating that corrosion rate is clearly related with *X*. This result indicates that corrosion inhibition ability of metal cations is increased with increasing *X* in 0.5 M Cl^- aqueous solution.

The corrosion inhibition efficiency of metal cations was calculated using equation (1) which were based on the mass loss due to immersion in the solutions.

$$\text{Corrosion inhibition efficiency } (\%) = \frac{\mathrm{Na_{ms}} - \mathrm{CAT_{ms}}}{\mathrm{Na_{ms}}} \times 100 \quad (1)$$

Where Na_{ms} is mass loss of specimen in Na_{sol} and CAT_{ms} is mass loss of specimen in solutions.

Fig. 3 shows the corrosion inhibition efficiency of metal cations as a function of *X* in which mean value of mass loss data was used. In this experiment Na_{sol} was used as a reference solution. Therefore, the corrosion inhibition efficiency of Na^+ was considered zero. The corrosion inhibition efficiency of Al^{3+} and Zn^{2+} are around 20% and 17% respectively.

The pH of the test solutions before and after immersion tests at 25°C for 56 d are shown in Table 1, pH_{int} is the pH of solutions before immersion tests, pH_{corr} is the pH obtained after the immersion tests. The pH was slightly decreased after immersion (pH_{corr}) in all solutions for 56 d (8 weeks) (Table 1). Several researchers also reported that the solution pH decreases with the hydrolysis of Fe^{2+} and Fe^{3+} [35, 36]. Additionally, proton is released into the solution during deprotonation of the passive films on the stainless steel surface in presence of metal cations [24] and thus pH of solutions is decreased.

The changes in the surface morphology of specimen were observed after the immersion tests. Fig. 4 shows the surface SEM images of specimens. The SEM images exhibit the huge numbers of pits in Na_{sol} and Mg_{sol}. Many pits depict the severe corrosion occurred on the

SUS304 surface. A few small pits are observed in the case of Zn_{sol} and Al_{sol}. However, comparatively smooth surface is observed in both Zn_{sol} and Al_{sol}. It suggests that specimen surface may be affected by the metal cations in the case of Zn_{sol} and Al_{sol}. These results correspond well to the mass change of specimen after immersed in the solutions.

3.2 Surface analysis

The specimen surfaces were examined by XPS after the immersion tests to clarify the effect of metal cations on the surface. Fig. 5 shows the XPS wide spectra of specimen immersed in the solutions. In the case of specimen immersed in Zn_{sol}, clear peak of Zn2p3/2 is observed indicating the presence of Zn on the specimen surface [23, 37]. In the case of specimen immersed in Al_{sol}, clear peak of Al2p3/2 is observed indicating the presence of Al on the specimen surface [23, 38]. From Fig. 5, there are no peaks of Cl2p3/2 (at 200 eV) observed on the specimens immersed in the solutions meaning that chlorine does not exist on the surface. This result suggests that chlorine was unable to form chemical bond with the corrosion inhibiting species.

The XPS depth analyses were carried out to determine how the metal elements were distributed or incorporated in the passive films. There are no peaks observed of Na1s and Mg1s on the specimen in the wide spectra (Fig. 5). However, XPS narrow spectra with depths of Na1s and Mg1s along with Zn2p3/2 and Al2p3/2 were carried out (due to low resolution of wide spectra) to determine the specific depth locations of each element and chemical state. Fig. 6 shows the XPS narrow spectra of Na1s, Mg1s, Zn2p3/2 and Al2p3/2 with depths of specimen surface after the immersion tests. Fig. 6 (a) and (b) show the Na1s and Mg1s spectra with depths of specimen immersed in Na_{sol} and Mg_{sol} respectively. From 0 nm to 16 nm depth, no peaks of both Na1s and Mg1s are observed. These results signify that both Na and Mg did not exist on the surface. Fig. 6 (c) shows the Zn2p3/2 spectra with depths of specimen immersed in Zn_{sol}. Peaks are observed at 1022.6 eV from 0 nm to 6 nm

depth which are related to the peak of Zn^{2+} [21, 23]. Fig. 6 (d) shows the Al2p3/2 spectra with depths of specimen immersed in Al_{sol}. Peaks are observed at 74.4 eV from 0 nm to 16 nm depth which are related to the peak of Al^{3+} [23].

Fig. 7 shows the narrow spectra with depths of Fe2p3/2, O1s and Cr2p3/2 of specimen immersed in the Zn_{sol} and Al_{sol}. Fig. 7 (a) and (b) show the Fe2p3/2 spectra with depths of specimen immersed in the Zn_{sol} and Al_{sol} respectively. In both case, peaks are observed at 707.05 eV which are related to the peak of Fe [39]. The peak intensity of Fe is increased with increasing the depth. Very small peaks are appeared at 710.2 eV and at 711.2 eV which are related to the peaks of Fe^{2+} and Fe^{3+} respectively [39]. In both case, the peak of metallic iron, and the peaks of Fe^{2+} and Fe^{3+} on the surface are negligible. Fig. 7 (c) and (d) show the Cr2p3/2 spectra with depths of specimen immersed in Zn_{sol} and Al_{sol} respectively. Both of the case, peaks are observed at 574.4 eV from 0 nm to 16 nm depth which are related to the peak of Cr [40]. Peaks are also observed at 576.9 eV from 0 nm to 6 nm depth which are related to the peak of Cr^{3+} [40], and high intensity is noticed from 0 nm to 1 nm depth. Fig. 7 (e) and (f) show the O1s spectra with depths of specimen immersed in Zn_{sol} and Al_{sol} respectively. Both of the case, peaks are observed and it can be separated into two peaks, one peak at 530.6 eV which is related to the peak of O^{2-} [39, 40], and another peak at 531.8 eV which is related to the peak of OH^- [39, 40].

From the XPS results of Fig. 6 and Fig. 7, it is demonstrated that both Zn^{2+} and Al^{3+} were existed on the surface and the peaks of these cations were related to the peaks of $Zn(OH)_2$ and $Al(OH)_3$ respectively [21, 23, 37, 38]. From the previous report, mild steel in Cl^- aqueous solution [21-23], metal cation made a chemical bond with the passive films and formed a metal cation layer which inhibited the corrosion reactions and protected the dissolution of metal. Therefore, it is expected that Zn^{2+} and Al^{3+} were existed on the surface as hydroxides and it further formed a chemical bond with the passive films by de-

hydroxylation process which were leaded to metal cation layer on the surface of SUS304 in the solution [24]. The metal cation layer would have good protective ability against the Cl^- attack in the solution and inhibits the corrosion reactions of SUS304. XPS quantification data of surface (0 nm) are shown in the Table 4. Higher atomic percentage of Al2p3/2 (24.17) is observed than the atomic percentage of Zn2p3/2 (14.96). These results suggest that Al^{3+} was distributed more than Zn^{2+} on the surface layer, and consequently the specimen immersed in the Al_{sol} showed lower corrosion rate than the specimen immersed in the Zn_{sol} (as showed in Fig. 2).

The surface roughness was measured by atomic force microscope and the recorded 3D images of surface topography are shown in Fig. 8. These images show different rough surface of specimen immersed in the solutions with metal cation. Comparatively smooth surface is observed of specimen immersed in the Al_{sol}. To quantify the surface roughness, mean roughness factor (R_a) [41, 42] was determined from the respective images. The calculated R_a values are shown in the Table 2. The roughness of the specimen surface was increased due to immersion in the solutions. However, the roughness of specimen immersed in the Al_{sol} shows the lowest value than other solutions indicating the metal cation layer formation on the specimen surface. These results correspond well to the surface morphological change observed by SEM.

3.3 Electrochemical tests

The open circuit potentials of SUS304 were measured in solutions and are shown in the Fig. 9. All the measured values are confined between -0.15 V and -0.25 V. Only slight difference is observed in the case of Mg_{sol}, Zn_{sol}, and Al_{sol} as compared to the Na_{sol}. However, after 3000 s, Na_{sol} induces the most negative open circuit potential.

Fig. 10 shows the cathodic and anodic polarization curves. From the cathodic polarization curves, it is found that Zn_{sol} and Al_{sol} shows lower current density (indicated by arrow in Fig.

10) and slightly acts as cathodic inhibitor as compared to the Na_{sol} and Mg_{sol}. In the anodic polarization curves, current density is increasing with increasing the potential in all the solutions. After at a certain potential, current density is increased suddenly and that potential is mentioned as pitting potential. Na_{sol} shows the lowest pitting potential as compared to the other solutions, and Zn_{sol} and Al_{sol} show lower current density (indicated by arrow in Fig. 10) as compared to the Na_{sol} and Mg_{sol}. These results suggest that both Zn_{sol} and Al_{sol} act as a cathodic and anodic inhibitor.

EIS measurements were carried out to clarify the initial corrosion behavior of the SUS304 and the effect of metal cations on the properties of the passive film. Fig. 11 (a) shows the impedance plots and Fig. 11 (b) shows the phase shift plots (Bode diagram) of the specimen in different solutions with metal cations. The impedance and phase shift show different magnitude in each solution with metal cations. The fitted lines are calculated by Randle's equivalent circuit model (Fig. 11 (c)) [43-45]. All the experimental spectra can be well described by this equivalent circuit. The equivalent circuit model consists of solution resistance (R_{sol}), charge-transfer resistance (R_{ct}), and constant phase element (CPE), Q. The calculated [46-49] mean values of electrochemical impedance parameters are listed in the Table 3. Q represents the structure of solution/metal interface and the area of defects in the protective film on the surface [22, 50]. Otani et. al [22] reported that the decrease in Q value indicates that Zn^{2+} can decrease the defect in the protective film on the mild steel. From the Table 3, lower value of Q is observed in Zn_{sol} and Al_{sol} as compared to the Na_{sol} and Mg_{sol}. Therefore, it is expected that the specimen immersed in Zn_{sol} and Al_{sol} have relatively perfect film as compared to the film formed on the specimen immersed in the Na_{sol} and Mg_{sol}.

The magnitude of impedance at low frequencies in Bode diagram implies the corrosion resistance of the SUS304 in the solution. Zn_{sol} and Al_{sol} show the larger magnitude of impedance at lower frequency (Fig. 11 (a)) as compared to the Mg_{sol} and Na_{sol}. Larger phase

shift also observed at lower frequency for both Zn_{sol} and Al_{sol} as compared to the Mg_{sol} and Na_{sol} (Fig. 11 (b)). These results suggest that both Zn^{2+} and Al^{3+} have the corrosion inhibitory effect on SUS304 in 0.5 M Cl^- aqueous solution. The results obtained from the electrochemical tests are in good agreement with the results from the immersion tests and surface analysis.

The values of R_{ct} as a function of *X* are shown in Fig. 12 (a). The R_{ct} increases with increasing the value of *X*, and the correlation coefficient is 0.92, signifying that R_{ct} is closely related with *X*. High R_{ct} indicates that charge transfer rate is low and the steel has high corrosion resistance in the solution. It signifies that Zn_{sol} and Al_{sol} expose higher corrosion resistance than Na_{sol} and Mg_{sol}. Fig. 12 (b) shows the changing of R_{ct} with mass loss of specimen immersed in the solutions in which mean values of both parameters have been used. Al_{sol} shows the highest R_{ct} than other solutions, and Al_{sol} has the lowest mass loss than other solutions with metal cation. This result indicates that the solutions with metal cations which have large *X*, exhibit higher R_{ct} and consequently implies the lower mass loss in the solution. The correlation coefficient is -0.98 indicating that R_{ct} and mass loss are closely related to each other.

4. Discussions

The present results shown in the above sections indicate that the harder metal cations played an important role of suppressing the corrosion initiation process by forming a layer on the passive films. It is expected that both zinc and aluminium may form a chemical bond with the passive films by de-hydroxylation process [24]. The formation of hydroxides and de-hydroxylation process are depended on the metal cation hardness, *X* [23]. Metal cations with large *X* are able to form a layer on the steel surface. The mechanism of which the metal cations with large *X* form a layer on the surface and suppress the corrosion reactions will be

discussed below based on the passive films model proposed by Okamoto and Shibata [51-53] and the HSAB concept [27, 54, 55] (Fig. 13).

Okamoto and Shibata proposed the following passive film model for stainless steels [51-53]. The passive films of stainless steel contain huge amount of bound water which are connected with the metal atoms and oxygen atoms. The atoms are arranged in the passive films like a bridge on the steel surface (Fig. 13 (a)). When the passive films on the stainless steel surface is ruptured by Cl^-, re-passivation process takes place immediately [56-58].

According to the HSAB concept, metal cations with large *X* incorporate in the passive films and attract the electron pair of oxygen atom in H_2O or OH^- in the passive films, and finally stimulates the deprotonation process (Fig.13 (b)). It is considered that the protons are replaced with the hard metal cations and form a metal cation layer on the passive films (Fig. 13 (c)). The layer of metal cation protects the passive films from Cl^- attack and inhibits the corrosion reactions of stainless steel. On the other hand, metal cations with small *X*, do not have the ability to make a layer with the passive films, and thus Cl^- can arrive on the metal surface by destroying the passive films and initiate the metal dissolution reactions.

5. Conclusions

- The corrosion behavior of the stainless steel in the 0.5 M Cl^- aqueous solution was changed with *X*, and corrosion rates were closely correlated with *X*.
- Different surface morphologies were observed by SEM after immersion in the solutions which were depended on the metal cations.
- Zn_{sol} and Al_{sol} showed higher impedance and higher charge transfer resistance as compared to Na_{sol} and Mg_{sol}.
- From the XPS results, Zn^{2+} and Al^{3+} were existed on the steel surface as hydroxides and formed a layer by incorporating in the passive films through de-hydroxylation process.

- The layer of metal cation would have good protecting ability against Cl^- attack as well as corrosion reactions on the steel surface.

Acknowledgements

This study was supported by the Salt Science Research Foundation [grant number 1609]. SEM and AFM observation of this work was conducted at the Laboratory of XPS analysis, Joint-use facilities, Hokkaido University, supported by "Material Analysis and Structure Analysis Open Unit (MASAOU). XPS analysis was conducted at the Laboratory of XPS analysis, Hokkaido University, supported by 'Nanotechnology Platform' Program of the Ministry of Education, Culture, Sports, Science and Technology (MEXT), Japan.

References

[1] P. D. Krell, S. Li and H. Cong, Synergistic effect of temperature and HCl concentration on the degradation of AISI 410 stainless steel, Corros. Sci., 122 (2017) 41-52.

[2] T. Takei, M. Yabe and F. G. Wei, Effect of cooling condition on the intergranular corrosion resistance of UNS S32506 duplex stainless steel, Corros. Sci., 122 (2017) 80-89.

[3] K. S. Raja muthu kumar, P. Vijian, J. Samu Solomon, L. John Berchmans, Corrosion studies on stainless steel-304 in brackish environment, Int. J. of Emerging Technology and Advanced Eng., 2 (2012) 178-182.

[4] S. Hastuty, A. Nishikata and T. Tsuru, Pitting corrosion of Type 430 stainless steel under chloride solution droplet, Corros. Sci., 52 (2010) 2035-2043.

[5] S. T. Kim, S. H. Jeon, I. S. Lee and Y. S. Park, Effects of rare earth metals addition on the resistance to pitting corrosion of super duplex stainless steel - Part 1, Corros. Sci., 52 (2010) 1897-1904.

[6] X. Yu, S. Chen, Y. Liu and F. Ren, A study of intergranular corrosion of austenitic stainless steel by electrochemical potentiodynamic reactivation, electron back-scattering diffraction and cellular automaton, Corros. Sci., 52 (2010) 1939-1947.

[7] J. Kovac, C. Alaux, T. J. Marrow, E. Govekar and A. Legat, Correlations of electrochemical noise, acoustic emission and complementary monitoring techniques

during intergranular stress-corrosion cracking of austenitic stainless steel, Corros. Sci., 52 (2010) 2015-2025.

[8] M. Behpour, S. M. Ghoreishi, M. Khayat Kashani and N. Soltani, Inhibition of 304 stainless steel corrosion in acidic solution by ferula gumosa (galbanum) extract, Mat. and Corros., 60 (2009) 895-898.

[9] J. Starosvetsky, D. Starosvetsky, B. Pokroy, T. Hilel, R. Armon, Electrochemical behavior of stainless steels in media containing iron-oxidizing bacteria (IOB) by corrosion process modeling, Corros. Sci., 50 (2008) 540-547.

[10] S. J. Yuan, S. O. Pehkonen, Y. P. Ting, E. T. Kang, and K. G. Neoh, Corrosion behavior of Type 304 stainless steel in a simulated seawater-based medium in the presence and absence of aerobic pseudomonas NCIMB 2021 bacteria, Ind. Eng. Chem. Res. 47 (2008) 3008-3020.

[11] Z. S. Smialowska and J. Mankowski, Crevice corrosion of stainless steels in sodium chloride solution, Corros. Sci., 18 (1978) 953-960.

[12] C. O. A. Olsson and D. Landolt, Passive films on stainless steels-chemistry, structure and growth, Electrochim. Acta 48 (2003) 1093-1104.

[13] G. Okamoto, Passive film of 18-8 stainless steel structure and its function, Corros. Sci., 13 (1973) 471-489.

[14] E. McCafferty, Introduction to corrosion science, Springer, 2010, pp. 283-286.

[15] T. Shibata, Passivity breakdown and stress corrosion cracking of stainless steel, Corros. Sci., 49 (2007) 20-30.

[16] L. A. Krebs and J. Kruger, International symposium; 8th, passivity of metals and semiconductors, Electrochem. Soc., Pennington, NJ, 2001, pp. 561-569.

[17] T. Shibata, Stochastic studies of passivity breakdown, Corros. Sci., 31 (1990) 413-423.

[18] N. Sato, An overview on the passivity of metals, Corros. Sci., 31 (1990) 1-19.

[19] D. D. Macdonald and M. U. Macdonald, Deterministic models for passivity breakdown, Corros. Sci., 31 (1990) 424-430.

[20] R. Nishimura and K. Kudo, The effects of passive films formed on iron, nickel and austenitic stainless steels (SUS 304 and SUS 316) on pitting corrosion, Corros. Sci., 31 (1990) 479-484.

[21] Md. S. Islam, K. Otani and M. Sakairi, Effects of metal cations on mild steel corrosion in 10 mM Cl^- aqueous solution, Corros. Sci., 131 (2018) 17-27.

[22] K. Otani, Md. S. Islam and M. Sakairi, Inhibition ability of gluconates for fresh water corrosion of mild steel enhanced by metal cations, J. Electrochem. Soci., 164 (2017) C498-C504.

[23] K. Otani, M. Sakairi, Effects of metal cations on corrosion of mild steel in model fresh water, Corros. Sci., 111 (2016) 302-312.

[24] S. Zhang, T. Shibata, T. Haruna, Inhibition of metal cations to intergranular stress corrosion cracking of sensitized Type 304 stainless steel, Corros. Sci., 47 (2005) 1049-1061.

[25] M. G. A. Khedr and A. M. S. Lashien, The role of metal cations in the corrosion and corrosion inhibition of aluminium in aqueous solutions, Corros. Sci., 33 (1992) 137-151.

[26] S. Tsujikawa and S. Okayama, Repassivation method to determine critical conditions in terms of electrode potential, temperature and NaCl concentration to predict crevice corrosion resistance of stainless steels, Corros. Sci., 31 (1990) 441-446.

[27] K. E. Heusler, Growth and dissolution of passivating films, Corros. Sci., 31 (1990) 597-606.

[28] C. S. O'dell, B. F. Brown, R. T. Foley, An exploratory study of inhibition of intergranular stress corrosion cracking in sensitized Type 304 stainless steel, Corrosion, 36 (1980) 183-200.

[29] D. M. Drazic and L. Z. Vorkapic, Inhibitory effects of manganeous, cadmium and zinc ions on hydrogen evolution reaction and corrosion of iron in sulphuric acid solutions, Corros. Sci., 18 (1978) 907-910.

[30] H. C. Gatos, Effects of metal cations on the corrosion of iron in acids, Corrosion, 12 (1956) 32-40.

[31] J. N. Esposito, G. Economy, W. A. Byers, J. B. Esposito, F. W. Pement, R. J. Jacko, C. A. Bergmann, in: Proc. 5th Int. Sympo. Environmental degradation of materials in nuclear power systems-water reactors, American Nuclear Society, 1992, pp. 495-503.

[32] C. J. Wood, W. J. Marbel, M. Prystupa, M. J. Hudson, D. L. Wilkens, in: Proc. of 5th Inter. Conf. on Water chemistry of nuclear reactor systems, vol. 1, BNES, 1989, pp. 111-120.

[33] K. F. Ankinpelumi, Investigation the effect of pH level on corrosion rate, University of Lagos, Lagos, 2012.

[34] I. A. Ammar and S. Riad, Effect of pH on corrosion potentials, J. Phys. Chem., 62 (1958) 150-154.

[35] F. H. Sweeton and C. F. Baes Jr., The solubility of magnetite and hydrolysis of ferrous ion in aqueous solutions at elevated temperatures, J. Chem. Thermodynamics, 2 (1970) 479-500.

[36] L. N. Mulay and P. W. Selwood, Hydrolysis of Fe^{3+}: magnetic and spectrophotometric studies on ferric perchlorate solutions, J. Am. Chem. Soc., 77 (1955) 2693-2701.

[37] G. Deroubaix, P. Marcus, X-ray photoelectron spectroscopy analysis of copper and zinc oxides and sulphides, Surf. Interface Anal. 18 (1992) 39-46.

[38] J.A. Taylor, An XPS study of the oxidation of AlAs thin films grown by MBE, J. Vac. Sci. Technol. 20 (1982) 751-755.

[39] K. Song, Y. Lee, M. R. Jo, K. M. Nam and Y. M. Kang, Comprehensive design of carbon- encapsulated Fe_3O_4 nanocrystals and their lithium storage properties, Nanotechnology 23 (2012) 505401-505406.

[40] S. Ningshen, M. Sakairi, K. Suzuki and S. Ukai, The corrosion resistance and passive film compositions of 12% Cr and 15% Cr oxide dispersion strengthened steels in nitric acid media, Corros. Sci., 78 (2014) 322-334.

[41] R. R. L. De Oliveira, D. A. C. Albuquerque, T. G. S. Cruz, F. M. Yamaji and F. L. Leite, Measurement of the nanoscale roughness by atomic force microscopy: Basic principles and applications, Federal University of São Carlos, Campus Sorocaba, Brazil, (2011) 147-174.

[42] A. K. Satapathy, G. Gunasekaran, S. C. Sahoo, Kumar Amit, P. V. Rodrigues, Corrosion inhibition by justicia gendarussa plant extract in hydrochloric acid solution, Corros. Sci., 51 (2009) 2848-2856.

[43] I. Martinez, C. Andrade, Application of EIS to cathodically protected steel: tests in sodium chloride solution and in chloride contaminated concrete, Corros. Sci., 50 (2008) 2948-2958.

[44] A. Popova, M. Christov, A. Vasilev, Inhibitive properties of quaternary ammonium bromides of N-containing heterocycles on acid mild steel corrosion. Part II: EIS results, Corros. Sci., 49 (2007) 3290-3302.

[45] D. A. Lopez, S. N. Simison and S. R. de Sanchez, Inhibitors performance in CO_2 corrosion EIS studies on the interaction between their molecular structure and steel microstructure, Corros. Sci., 47 (2005) 735-755.

[46] P. C. Torres, T. J. Mesquita and R. P. Nogueira, Relationship between the origin of constant-phase element behavior in electrochemical impedance spectroscopy and electrode surface structure, J. Phys. Chem. 119 (2015) 4136-4147.

[47] M. E. Orazem, I. Frateur, B. Tribollet, V. Vivier, S. Marcelin, Dielectric properties of materials showing constant-phase-element (CPE) impedance response. J. Electrochem. Soci., 160 (2013) C215-C225.

[48] B. Hirschorn, M. E. Orazem, B. Tribollet, V. Vivier, I. Frateur and M. Musiani, Determination of effective capacitance and film thickness from constant-phase-element parameters, Electrochim. Acta, 55 (2010) 6218-6227.

[49] G. J. Brug, A. L. G. Van Den Eeden, M. S. Rehbach and J. H. Sluyters, The analysis of electrode impedances complicated by the presence of a constant phase element, J. Electroanal Chem., 176 (1984) 275-295.

[50] M. Mahdavian and R. Naderi, Corrosion inhibition of mild steel in sodium chloride solution by some zinc complexes, Corros. Sci., 53 (2011) 1194-1200.

[51] G. Okamoto, T. Shibata, in: R. P. Frankenthal, J. Kruger (Eds.), Proc. of Passivity of Metals, The Electrochemical Society Inc., Princeton, NJ, 1978, pp. 646-677.

[52] G. Okamoto, T. Shibata, Stability of passive stainless steel in relation to the potential of passivation treatment, Corros. Sci., 10 (1970) 371-378.

[53] S. Ahrland, J. Chatt, N. R. Davies, The relative affinities of ligand atoms for acceptor molecules and ions, Quart. Rev. London, 12 (1958) 265-276.

[54] G. Okamoto, T. Shibata, Desorption of tritiated bound-water from the passive film formed on stainless steels, Nature, 206 (1965) 1350.

[55] R. G. Pearson, Hard and soft acids and bases, J. Am. Chem. Soc., 85 (1963) 3533-3539.

[56] M. Haginuma, S. Ono, M. Sambongi, K. Takeda, K. Tachibana, K. Ishigure, in: Proc. of 1998 JAIF Inter. Conf. on Water Chem. in Nuclear Power Plants, Japan Atomic Industrial Forum, Inc., 1998, pp. 122-129.

[57] T. M. Angeliu, P. L. Andresen, Effect of zinc additions on oxide rupture strain and re-passivation kinetics of iron-based alloys in 288°C water, Corrosion, 52 (1996) 28-35.

[58] L. W. Niedrach, W. H. Stoddard, Effect of zinc on corrosion films that form on stainless steel, Corrosion, 42 (1986) 546-549.

Captions

Table 1 The pH of the solutions used for immersion tests, initial value (pH_{int}), after immersion of specimens (pH_{corr}).

Table 2 AFM surface roughness data of specimen immersed in the solutions with metal cation at 25°C for 56 d.

Table 3 The simulated mean values of electrochemical impedance parameters of SUS304 after immersion in the solutions for 7 d.

Table 4 XPS quantification data of specimen immersed in the solutions (atomic %).

Fig. 1 Appearance of (a) solutions and (b) specimens after immersed in the solutions at 25°C for 56 d.

Fig. 2 Corrosion rate as a function of *X*.

Fig. 3 Corrosion inhibition efficiency of metal cations as a function of *X*.

Fig. 4 Surface SEM images of specimen after immersion in the solutions at 25°C for 56 d.

Fig. 5 XPS wide spectra of specimen surface after immersion in the solutions.

Fig. 6 XPS narrow spectra of metal cations with depth a) Na1s peaks of specimen immersed in Na_{sol}, b) Mg1s peaks of specimen immersed in Mg_{sol}, c) Zn2p3/2 peaks of specimen immersed in Zn_{sol}, d) Al2p3/2 peaks of specimen immersed in Al_{sol}.

Fig. 7 XPS narrow spectra with depth a) Fe2p3/2 c) Cr2p3/2 and e) O1s peaks of specimen immersed in Zn_{sol}, b) Fe2p3/2 d) Cr2p3/2 and f) O1s peaks of specimen immersed in Al_{sol}.

Fig. 8 AFM 3D images of specimen immersed in the solutions at 25°C for 56 d.

Fig. 9 Open circuit potential after immersion for 7 d in the different solutions with metal cations.

Fig. 10 Polarization curves of specimen immersed in the different solutions with metal cations.

Fig. 11 Results of EIS in the solution with different metal cations after immersion for 7 d, Bode diagram of (a) Impedance and (b) phase shift plot, (c) equivalent circuit model used to fit the EIS data.

Fig. 12 (a) Changing of R_{ct} as a function of X, (b) Changing of R_{ct} with mass loss of specimen immersed in the solutions.

Fig. 13 (a) Schematic representation of the passive films structure with hard metal cations in 0.5 M Cl^- aqueous solution (M^{n+} = Zn^{2+}, Al^{3+}). (b) deprotonation process accelerated by hard metal cations, M^{n+}. (c) formation of metal cation layer on the passive films by hard metal cations.

Table 1 pH of the solutions used for immersion tests, initial value (pH_{int}), after immersion of specimens (pH_{corr}).

Test solutions	pH_{int}	pH_{corr}
Na_{sol}	5.8	4.3
Mg_{sol}	5.7	4.2
Zn_{sol}	5.7	4.3
Al_{sol}	5.7	4.5

Table 2 AFM surface roughness data of SUS304 immersed in the solutions with metal cation at 25°C for 56 d.

Solutions	Surface roughness average, R_a (nm)	
	Before immersion	After immersion
Na_{sol}	4.67	27.71
Mg_{sol}	4.62	13.69
Zn_{sol}	4.65	8.25
Al_{sol}	4.60	7.14

Table 3 The simulated mean values of electrochemical impedance parameters of SUS304 after immersion in the solutions for 7 d.

Solutions	R_{sol} (Ωcm^2)	R_{ct} ($M\Omega cm^2$)	Q ($\mu s^n \Omega^{-1} cm^{-2}$)	n
Na_{sol}	15.57	0.97	12.55	0.89
Mg_{sol}	15.28	1.18	9.05	0.91
Zn_{sol}	15.77	2.51	3.95	0.86
Al_{sol}	15.84	3.21	8.51	0.87

Table 4 XPS quantification data of specimen immersed in the solutions (atomic %)

Specimen immersed in solution	Fe2p3/2	O1s	Cr2p3/2	Zn2p3/2	Al2p3/2
Zn_{sol}	16.35	24.67	12.11	14.96	-
Al_{sol}	15.05	22.10	10.31	-	24.17

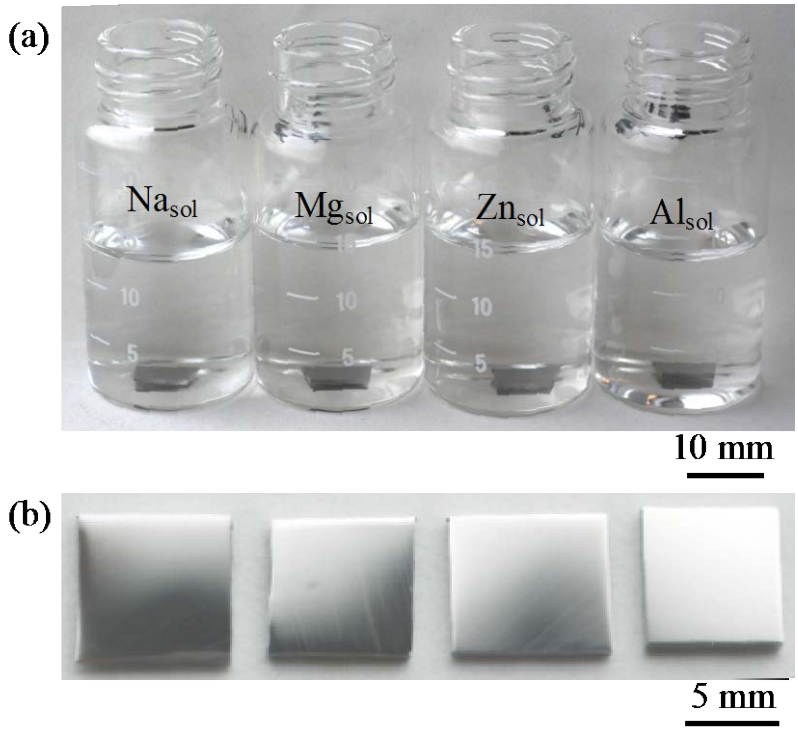

Fig. 1 Appearance of (a) solutions and (b) specimens after immersed in the solutions at 25°C for 56 d.

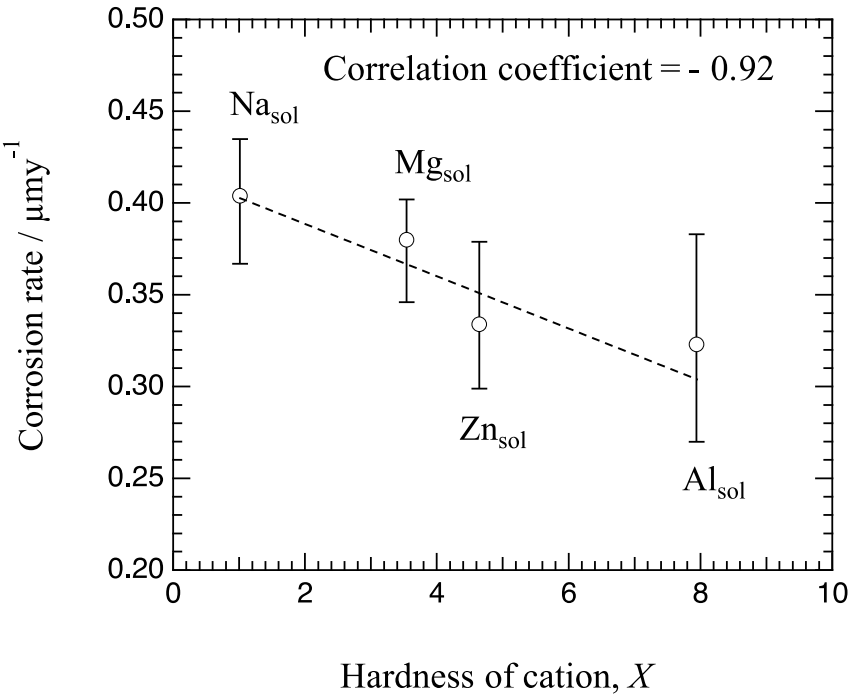

Fig. 2 Corrosion rate as a function of X.

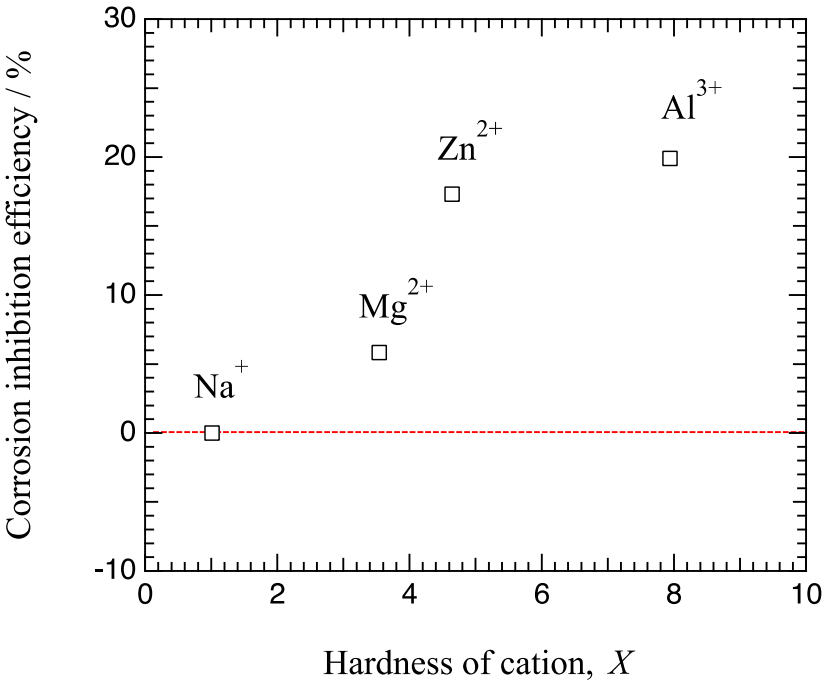

Fig. 3 Corrosion inhibition efficiency of metal cations as a function of *X*.

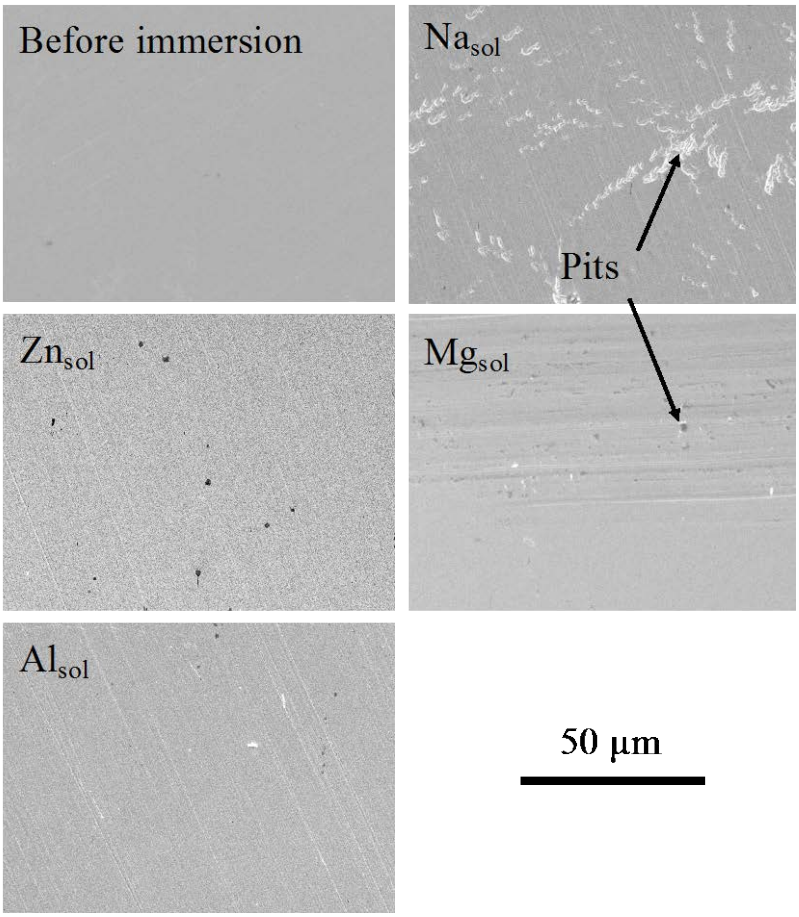

Fig. 4 Surface SEM images of specimen after immersion in the solutions at 25°C for 56 d.

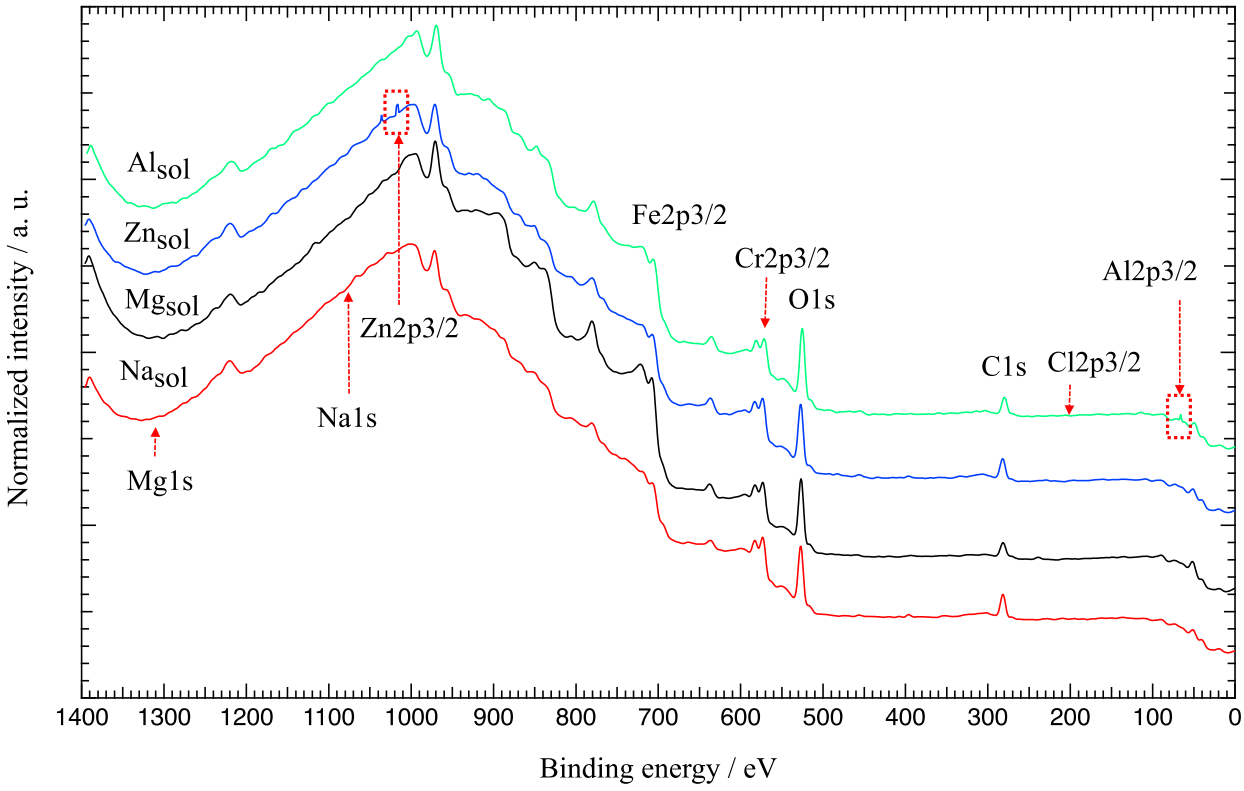

Fig. 5 XPS wide spectra of specimen surface after immersion in the solutions.

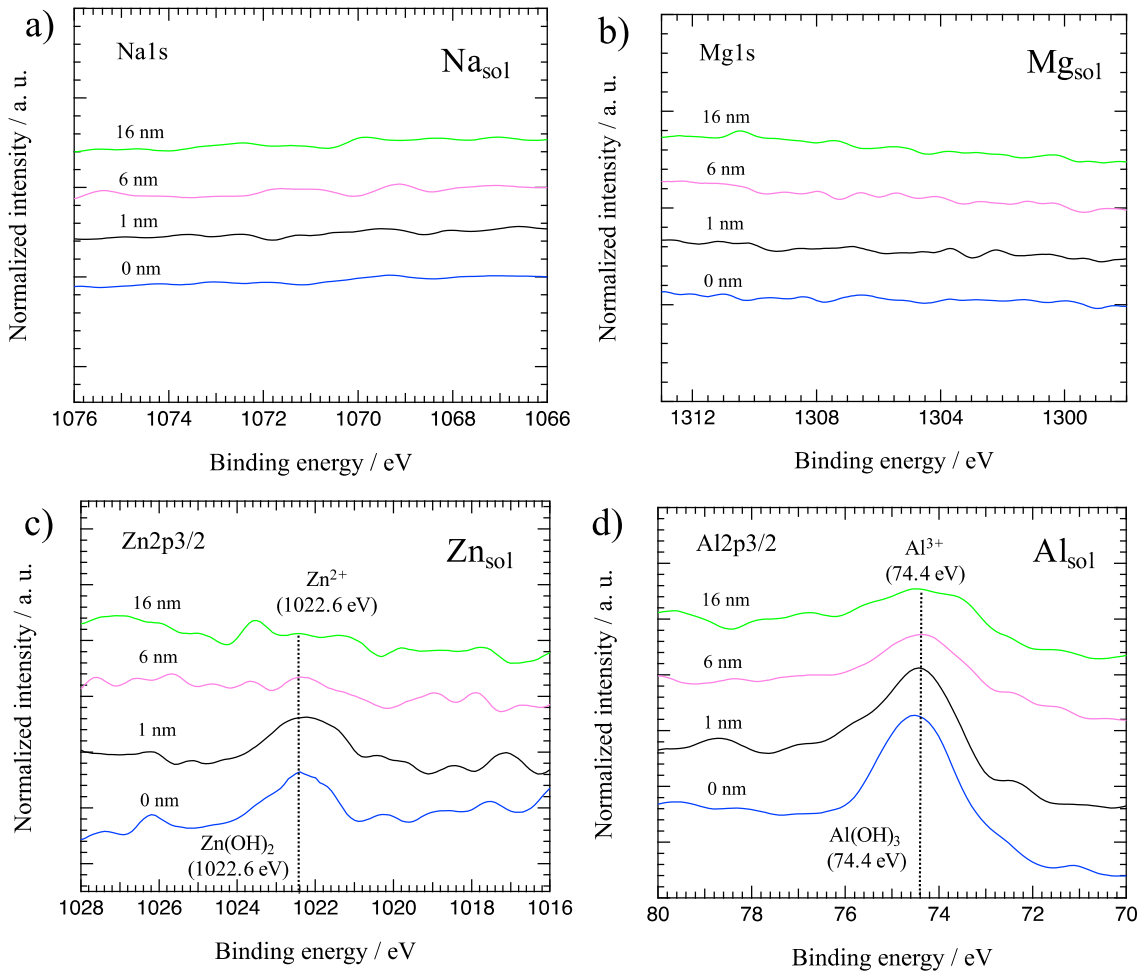

Fig. 6 XPS narrow spectra of metal cations with depth a) Na1s peaks of specimen immersed in Na_{sol}, b) Mg1s peaks of specimen immersed in Mg_{sol}, c) Zn2p3/2 peaks of specimen immersed in Zn_{sol}, d) Al2p3/2 peaks of specimen immersed in Al_{sol}.

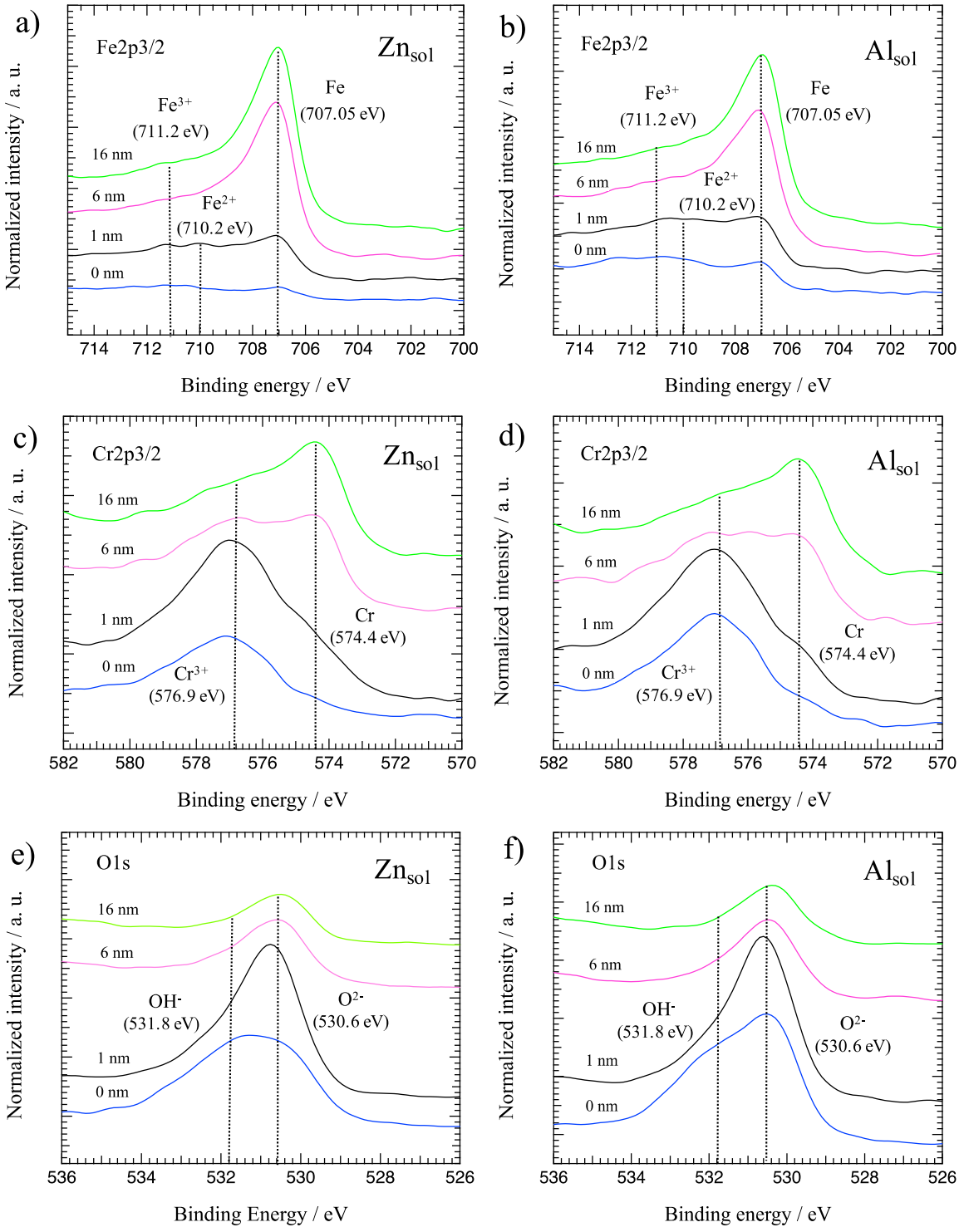

Fig. 7 XPS narrow spectra with depth a) Fe2p3/2 c) Cr2p3/2 and e) O1s peaks of specimen immersed in Zn_{sol}, b) Fe2p3/2 d) Cr2p3/2 and f) O1s peaks of specimen immersed in Al_{sol}.

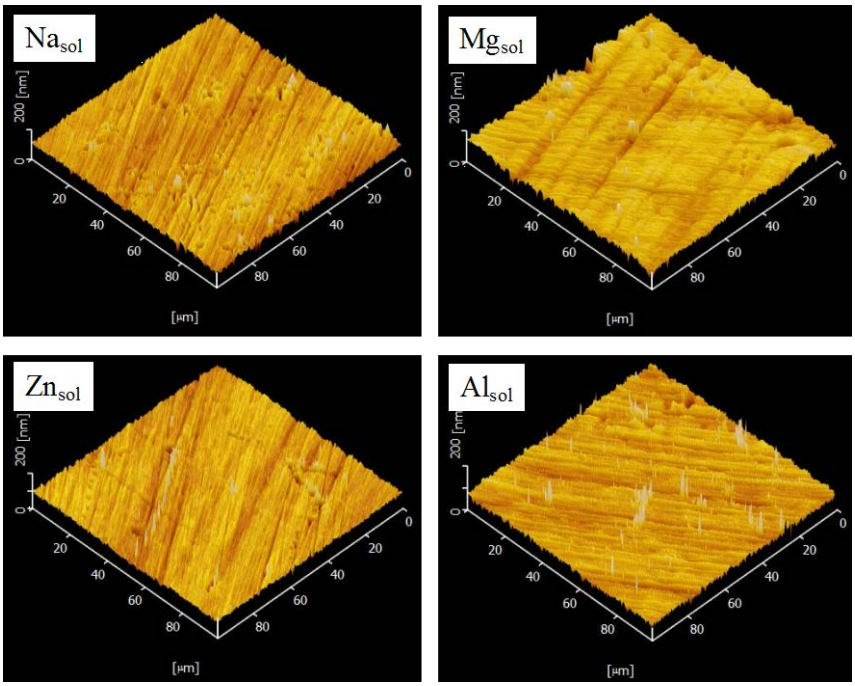

Fig. 8 AFM 3D images of specimen immersed in the solutions at 25°C for 56 d.

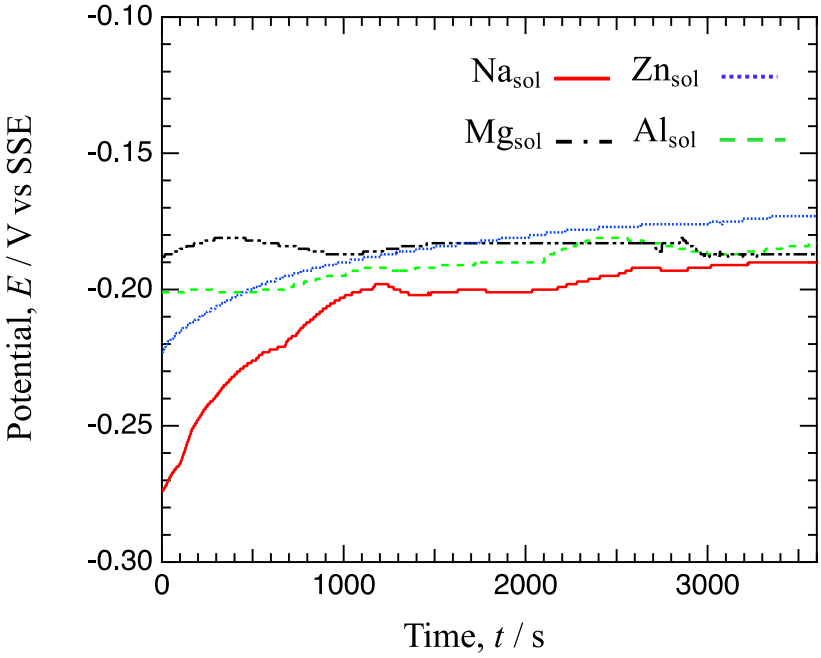

Fig. 9 Open circuit potential after immersion for 7 d in the different solutions with metal cations.

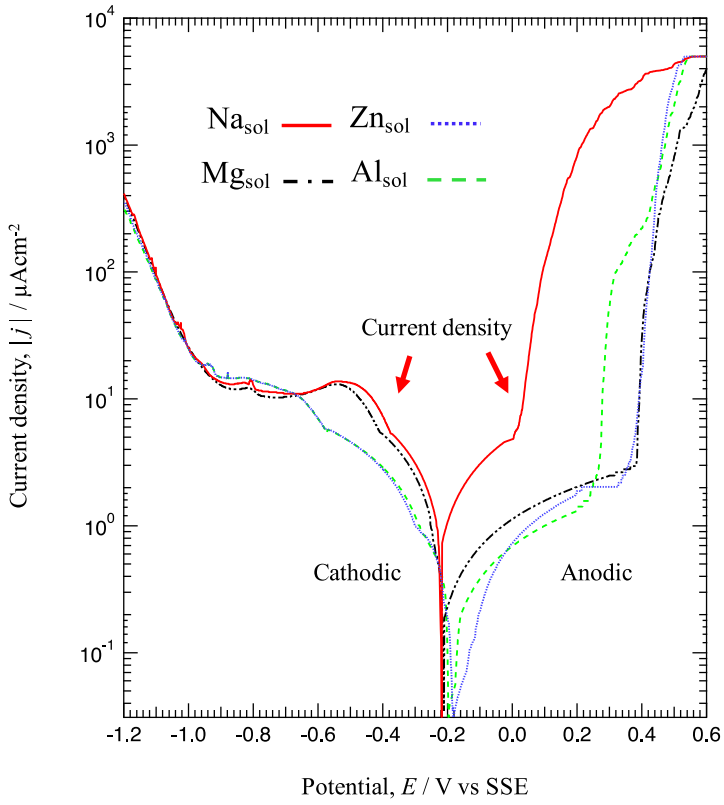

Fig. 10 Polarization curves of specimen immersed in the different solutions with metal cations.

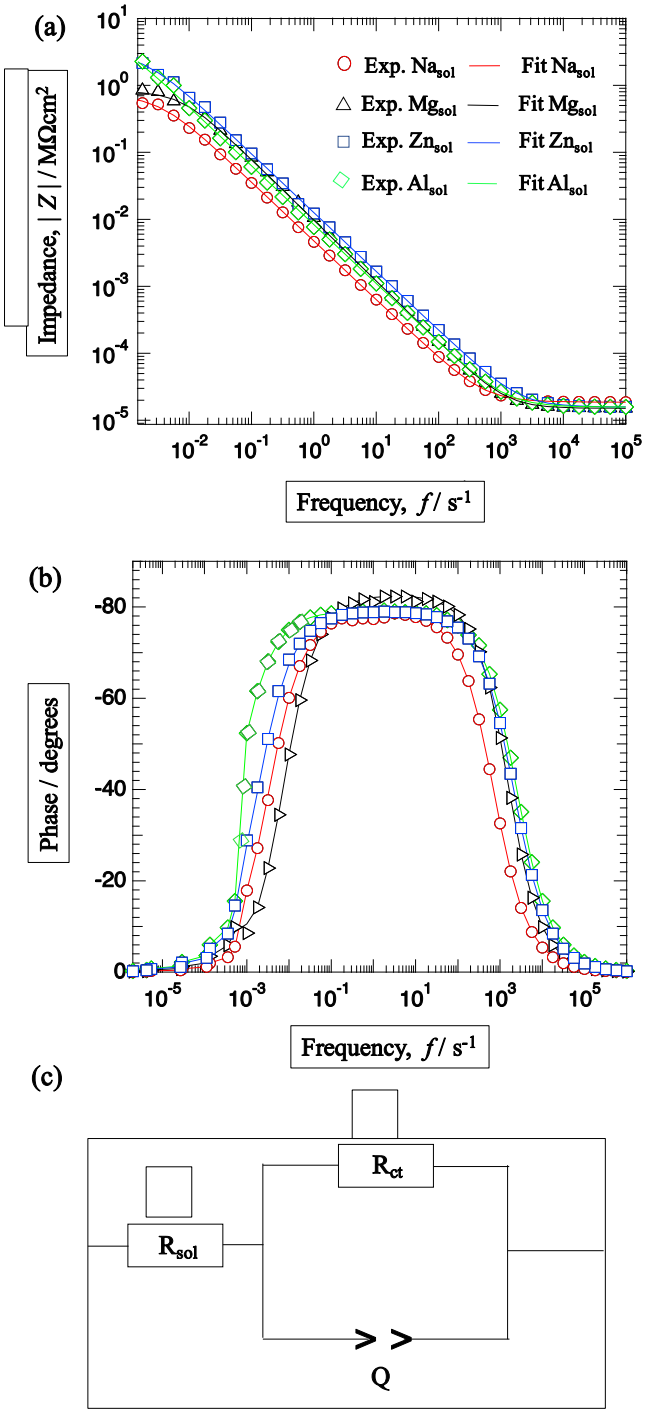

Fig. 11 Results of EIS in the solution with different metal cations after immersion for 7 d, Bode diagram of (a) Impedance and (b) phase shift plot, (c) equivalent circuit model used to fit the EIS data.

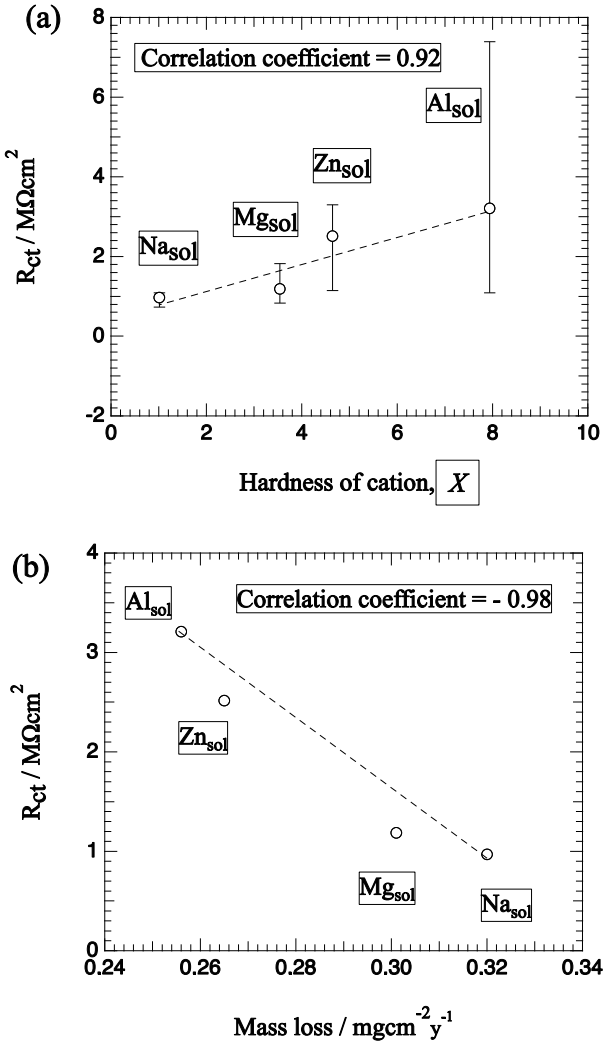

Fig. 12 (a) Changing of R_{ct} as a function of *X*, (b) Changing of R_{ct} with mass loss of specimen immersed in the solutions.

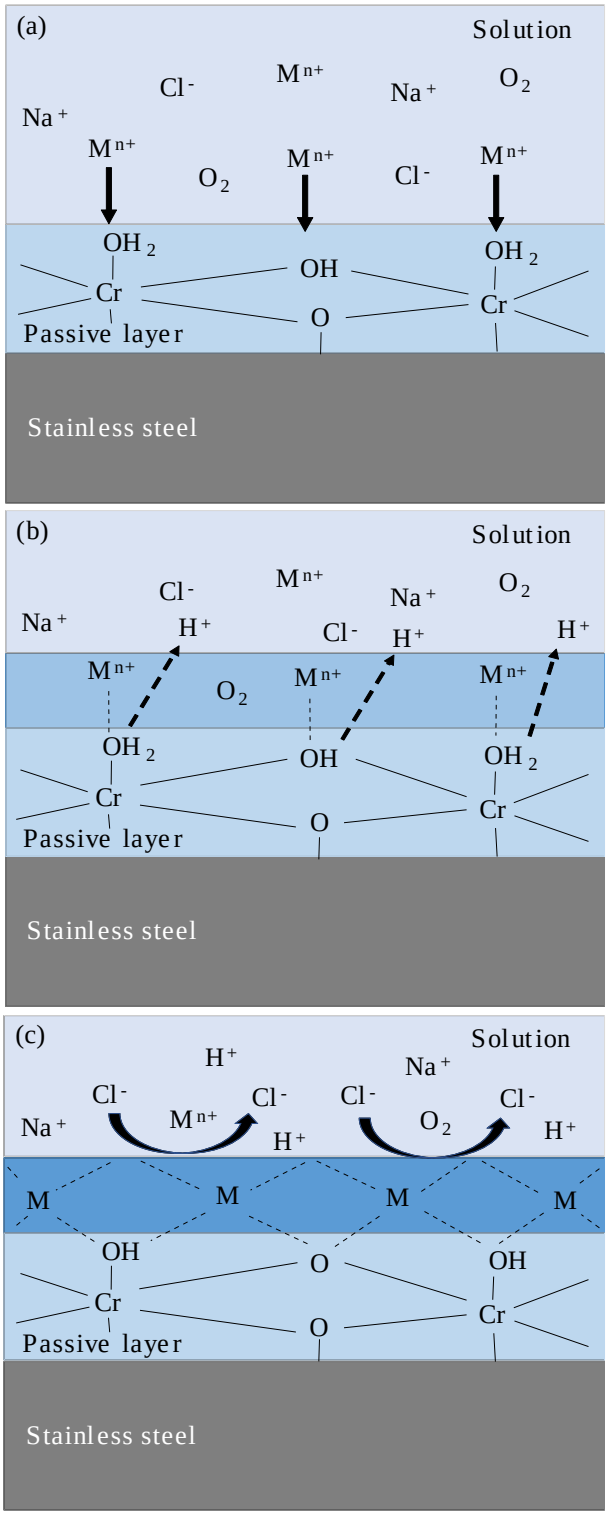

Fig. 13 (a) Schematic representation of the passive films structure with hard metal cations in 0.5 M Cl^- aqueous solution (M^{n+} = Zn^{2+}, Al^{3+}). (b) deprotonation process accelerated by hard metal cations, M^{n+}. (c) formation of metal cation layer on the passive films by hard metal cations.